Molecular Therapy
Methods & Clinical Development
Original Article

# Galactosialidosis: preclinical enzyme replacement therapy in a mouse model of the disease, a proof of concept

Jaclyn Cadaoas,[1] Huimin Hu,[2,3] Gabrielle Boyle,[1,3] Elida Gomero,[2,3] Rosario Mosca,[2,3] Kartika Jayashankar,[1] Mike Machado,[1] Sean Cullen,[1] Belle Guzman,[1] Diantha van de Vlekkert,[2] Ida Annunziata,[2] Michel Vellard,[1] Emil Kakkis,[1] Vish Koppaka,[1] and Alessandra d'Azzo[2]

[1]Ultragenyx Pharmaceutical, Novato, CA 94949, USA; [2]Department of Genetics, St. Jude Children's Research Hospital, 262 Danny Thomas Place, Memphis, TN 38105, USA

**Galactosialidosis is a rare lysosomal storage disease caused by a congenital defect of protective protein/cathepsin A (PPCA) and secondary deficiency of neuraminidase-1 and β-galactosidase. PPCA is a lysosomal serine carboxypeptidase that functions as a chaperone for neuraminidase-1 and β-galactosidase within a lysosomal multi-protein complex. Combined deficiency of the three enzymes leads to accumulation of sialylated glycoproteins and oligosaccharides in tissues and body fluids and manifests in a systemic disease pathology with severity mostly correlating with the type of mutation(s) and age of onset of the symptoms. Here, we describe a proof-of-concept, preclinical study toward the development of enzyme replacement therapy for galactosialidosis, using a recombinant human PPCA. We show that the recombinant enzyme, taken up by patient-derived fibroblasts, restored cathepsin A, neuraminidase-1, and β-galactosidase activities. Long-term, bi-weekly injection of the recombinant enzyme in a cohort of mice with null mutation at the *PPCA* (*CTSA*) locus (*PPCA*$^{-/-}$), a faithful model of the disease, demonstrated a dose-dependent, systemic internalization of the enzyme by cells of various organs, including the brain. This resulted in restoration/normalization of the three enzyme activities, resolution of histopathology, and reduction of sialyloligosaccharidiuria. These positive results underscore the benefits of a PPCA-mediated enzyme replacement therapy for the treatment of galactosialidosis.**

## INTRODUCTION

Galactosialidosis (GS) is a lysosomal glycoproteinosis caused by genetic deficiency of the serine carboxypeptidase, protective protein/cathepsin A (PPCA), which secondarily affects the activity and stability of two glycosidases: neuraminidase-1 (NEU1) and β-galactosidase (β-GAL).[1–4] Mammalian PPCA is a member of the serine protease family of enzymes and displays broad substrate specificity at both acidic and neutral pH.[5–9] It is synthesized as an enzymatically inactive 54-kDa precursor and proteolytically processed in lysosomes into a 32/20-kDa mature and active enzyme.[1,5,10] Distinct from its catalytic activity, PPCA has a protective, chaperone-like function toward NEU1 and β-GAL, with which it forms a high molecular weight complex.[2] In this configuration, the three enzymes acquire their stable conformation and full activity in lysosomes.[2,10–12] In the absence of a functional PPCA, NEU1 is no longer active, and β-GAL retains only 15%–20% of activity, with consequent accumulation of sialylated glycoproteins and oligosaccharides in tissues and body fluids.[4] The latter likely accounts for the broad spectrum of clinical manifestations observed in patients.[3,4,13]

GS patients are usually classified, based on the age of onset and degree of severity of their symptoms, into three clinical subtypes: early infantile, late infantile, and juvenile/adult.[4] The severe early infantile forms develop a systemic condition associated with fetal hydrops, skeletal dysplasia, visceromegaly, renal and cardiac failure, variable neurological involvement, and premature death. The late infantile forms comprise a distinct group of patients with mild or absent cognitive disability. Symptoms appear in early childhood and progress into adulthood. They include coarse facies, dysostosis multiplex, growth retardation, heart and kidney problems, and hearing loss. The majority of GS patients have the juvenile/adult form of the disease, and they are mostly of Japanese origin. In spite of the late onset of the symptoms and survival into adulthood, these patients have a more severe clinical presentation and develop neurological signs, myoclonus, cerebellar ataxia, seizures, and mental retardation. In most instances, GS patients are diagnosed by their combined NEU1/β-GAL deficiency and oligosaccharidiuria, prior to confirmation of the diagnosis by mutation analysis and cathepsin A activity.[3,4]

A mouse model of GS carrying a null mutation at the *PPCA* (*CTSA*) locus (*PPCA*$^{-/-}$) develops a phenotype resembling human patients with the early onset and severe form of GS.[3,14] Symptoms includes severe nephropathy, splenomegaly, progressive ataxia, and early death. This phenotype is accompanied by extensive lysosomal

Received 13 August 2020; accepted 17 November 2020;
https://doi.org/10.1016/j.omtm.2020.11.012.

[3]These authors contributed equally

**Correspondence:** Alessandra d'Azzo, Department of Genetics, St. Jude Children's Research Hospital, 262 Danny Thomas Place, Memphis, TN 38105, USA.
**E-mail:** sandra.dazzo@stjude.org

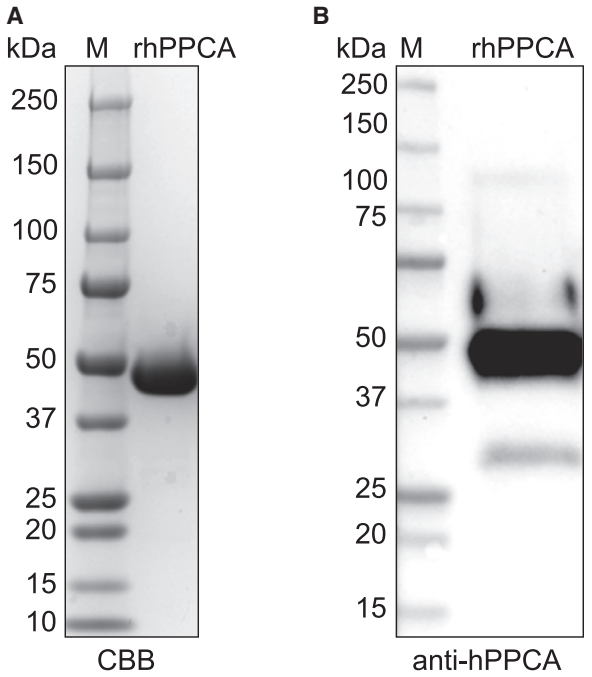


**Figure 1. SDS-PAGE analysis of rhPPCA under reducing conditions**
(A and B) Representative images showing the purity of rhPPCA on a Coomassie brilliant blue (CBB)-stained polyacrylamide gel (A) and on an immunoblot probed with anti-hPPCA antibody (B).

vacuolation and lysosomal expansion in cells of most systemic organs and the nervous system. *PPCA*$^{-/-}$ mice have no cathepsin A activity and low or undetectable NEU1 activity. However, in contrast to GS patients, β-GAL activity is partially reduced only in certain cells of young mice but tends to increase in most tissues, as the animals age.[14] This model has been extensively used for the *in vivo* assessment of various therapeutic modalities, including bone marrow transplantation, bone marrow-mediated *ex vivo* gene therapy, AAV (Adeno-associated virus)-mediated therapy, and enzyme replacement therapy (ERT).[14–18]

Here, we present the results of a proof-of-concept preclinical study that was performed in *PPCA*$^{-/-}$ mice to determine the therapeutic efficacy of ERT for the treatment of patients with GS. A recombinant human PPCA (rhPPCA) was expressed in Chinese hamster ovary (CHO) cells and purified from the culture medium. Uptake of rhPPCA by patient-derived fibroblasts showed that it was saturable, mannose-6-phosphate (M6P) receptor dependent, and restored the three enzyme activities. *PPCA*$^{-/-}$ mice injected intravenously with different doses of the purified rhPPCA showed a dose-dependent increase in cathepsin A activity in affected organs, diminished lysosomal vacuolation, and a reduction of urinary sialyloligosaccharides. This study unequivocally demonstrates the efficacy of rhPPCA in reverting the disease phenotype with no signs of associated toxicity, strongly encouraging the use of ERT for the treatment of GS patients, particularly those with a non-neuropathic disease.

## RESULTS

### rhPPCA production and biochemical properties

The rhPPCA used in this study was produced in CHO cells overexpressing the 54-kDa precursor form of human PPCA and purified from the culture medium with an overall purification recovery >30% and a specific activity of ∼132 mU/mg protein (Table S1). The final purity of rhPPCA was >95% when tested by SDS-PAGE under reducing conditions (Figures 1A and 1B). Some of the physical and functional characteristics of the purified rhPPCA are summarized in Table S1. On Coomassie-stained gels, the purified precursor appeared as a single band of ∼50 kDa (Figure 1A). Immunoblots of rhPPCA with anti-hPPCA antibody showed trace amounts (less than 2% of the protein) of the mature cathepsin A large chain of ∼30 kDa (Figure 1B). Differences in molecular weight between the recombinant enzyme generated in CHO cells and native human PPCA most likely reflect variation in glycan composition. This is in agreement with other CHO cell-produced lysosomal enzymes used for ERT.[19,20] Super elongation complex (SEC)-high-performance liquid chromatography (HPLC) data confirmed that the rhPPCA precursor was a noncovalently linked dimer under native conditions (Table S1).

### *In vitro* pharmacokinetics (PKs) of rhPPCA

#### *Uptake of rhPPCA by patient-derived GS fibroblasts restores NEU1 and β-GAL activities*

Delivery of soluble lysosomal enzymes to various cells/tissues following ERT depends on the presence of the M6P recognition marker on the enzyme precursors at the terminal ends of their *N*-linked glycans.[21] Analysis of the M6P content on *N*-linked glycans released from rhPPCA was ∼1.8 mol/mol PPCA (Table S1). To test whether M6P-containing rhPPCA was efficiently internalized by cells and delivered to the lysosomes, we performed a series of uptake studies using PPCA-deficient, patient-derived fibroblasts. We found that the recombinant precursor was taken up in a dose-dependent fashion, and the uptake was competitive and saturable, with a $K_{uptake}$ of 1−3 nM, and was inhibited by coincubation of the culture with M6P (Figures 2A and 2B). These results are consistent with other recombinant human enzymes used for ERT in the clinic (e.g., rh-iduronidase $K_{uptake}$ is 1−2 nM).[22]

Maturation of human PPCA occurs in two steps: an endoproteolytic cleavage of the 54-kDa precursor gives rise to a transient intermediate of 34 and 20 kDa, which is then converted into the 32/20-kDa mature enzyme by trimming of the last 14 amino acids at the COOH terminus of the large chain.[10,23,24] To test the intracellular maturation of the rhPPCA precursor *in vitro*, uptake experiments were performed in patient-derived GS fibroblasts, using normal human fibroblasts as a control. Upon uptake, the rhPPCA was correctly processed in lysosomes into the mature and catalytically active form of the enzyme. The dose-dependent increase in the 30-kDa mature form of the protein detected on immunoblots (Figure 2C) was paralleled by the increase in cathepsin A activity relative to the normal fibroblast control (Figure 2D). Uptake of rhPPCA was accompanied by restoration of NEU1 activity to levels similar to those observed in normal fibroblasts

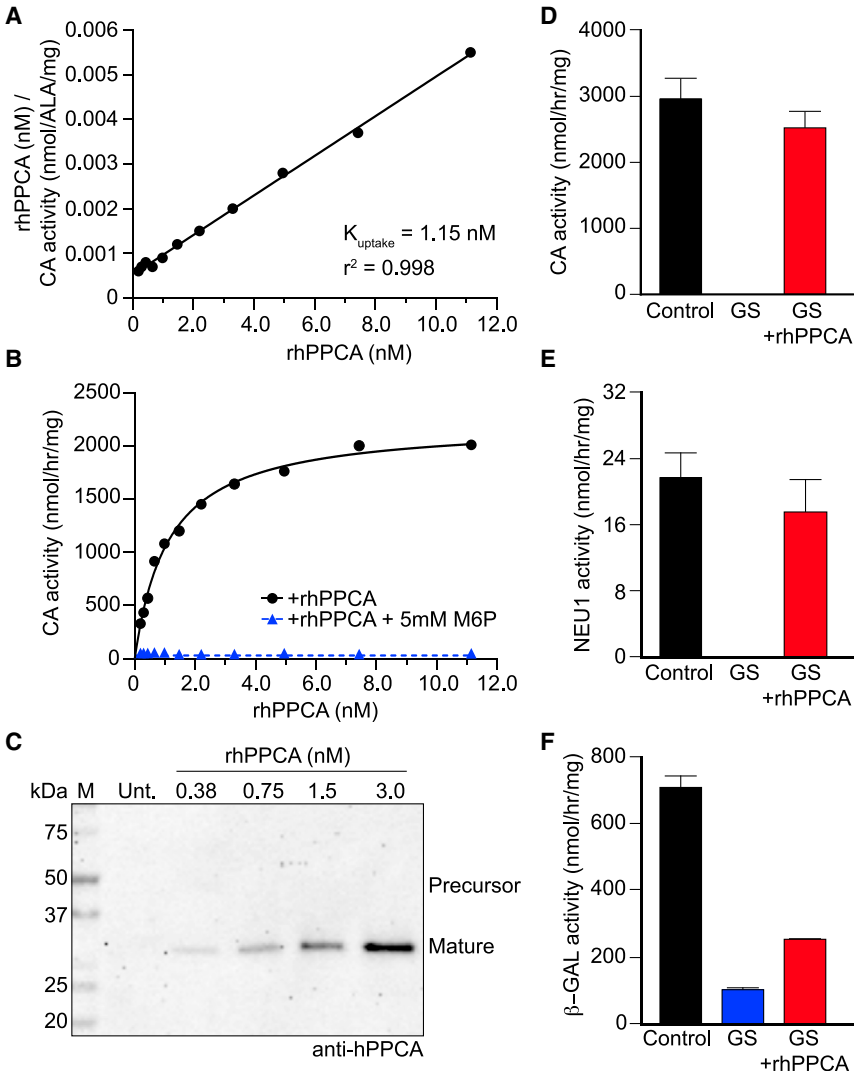


**Figure 2. rhPPCA is delivered to the lysosome in patient-derived GS fibroblasts**

(A) $K_{uptake}$ determination of rhPPCA by Hanes-Woolf regression analysis following 24 h uptake in GS fibroblasts. rhPPCA shows a high-affinity $K_{uptake}$ of 1–3 nM, n = 12. (B) Dose-dependent and receptor-mediated uptake of rhPPCA in the absence or presence of the competitive inhibitor, M6P, n = 11. (C) Immunoblot of lysates derived from GS fibroblasts treated with increasing amount of rhPPCA and probed with an anti-hPPCA antibody. Dose-dependent detection of ~30 kDa of the mature form of rhPPCA confirms the lysosomal delivery and conversion of the precursor into a mature and active form. (D–F) Cathepsin A (D), NEU1 (E), and β-GAL (F) activities performed in cell lysates following treatment with rhPPCA. Normal human fibroblasts were used as positive control, n = 3.

and by increased β-GAL activity (Figures 2E and 2F), a proof that the recombinant precursor was able to assemble into a three enzyme complex.

In order to determine the half-life of rhPPCA in rodent serum, urine, and tissues, as well as the terminal time points to be used in *PPCA*$^{-/-}$ mice, a single-dose (6-mg/kg) PK study was performed in 18 male Sprague-Dawley rats. Analysis of serum concentration of rhPPCA postintravenous dosing indicated consistent PK values among injected animals (Table S2). Levels of rhPPCA increased in all animals, with the time to reach the maximum serum concentration ($C_{max}$ [$T_{max}$]) at ~9 min postdose and declined thereafter with a half-life of ~14 min (Table S2). Similar PK parameters were assessed in tissues of injected rats (Table S3). The activity of cathepsin A was measured in tissues (liver, spleen, kidney, and lung) at different time points, and the half-life of the internalized enzyme was calculated to be between 10 and 23 h, depending on the tissues (Table S3). The activity in heart and brain tissue was close to background at all time points and could not be defined. In all tissues other than the brain, the $T_{max}$ was calculated to be at 2 h postdose (Table S3). Based on this information, the terminal time point for the mouse study was determined to be ~24 h post the last dose. Doses of rhPPCA to be injected in the mouse model were calculated based on the levels of recombinant enzyme in sera and the cathepsin A activity measured in tissues of injected rats, as well as the body weight of individual mice (Tables S2 and S3).

### In vivo *ERT with rhPPCA in GS mice*

Following a strictly standardized protocol (Table 1), an 8-week-long study was performed in a large cohort of *PPCA*$^{-/-}$ mice to assess the distribution, safety, and therapeutic efficacy of rhPPCA. *PPCA*$^{-/-}$ mice received rhPPCA by tail-vein injection, biweekly for 8 consecutive weeks (Table 1). To minimize a potential mounting of an immune response against rhPPCA, a common problem with ERT,[25] we included the administration of the antihistamine, cyproheptadine (CPH), 30 min prior to each injection. Following this regimen, only one animal was lost during the study, indicating that pretreatment with antihistamine was effective in preventing possible anaphylactic reactions to repeating doses of rhPPCA. No other significant clinical observations were noted. There were no detectable changes in the serum chemistry and hematology parameters, and all animals gained or maintained their weight over the course of the study in all treatment groups (Figure S1). Thus, rhPPCA was well tolerated in mice at doses up to 20 mg/kg, without evidence of toxic or pathological effects.

### *Dose-dependent changes in cathepsin A, NEU1, and β-GAL activities in tissues of* PPCA$^{-/-}$ *mice after 8 weeks of ERT*

To determine the distribution of rhPPCA following 8-week-long ERT, the liver, spleen, heart, kidney, brain, lung, quadriceps, and

**Table 1. Study design for mice receiving rhPPCA or vehicle treatment**

| Group # | Test article(s) | Gender[a] | Genotype | rhPPCA dose (mg/kg)[b] | Terminal collection time point (h)[c] |
|---|---|---|---|---|---|
| 1 (control) | vehicle | M/F | WT | 0 | 24 |
| 2 (control) | vehicle | M/F | *PPCA*$^{-/-}$ | 0 | 24 |
| 3 (control) | vehicle + CPH[d] | M/F | *PPCA*$^{-/-}$ | 0 | 24 |
| 4 | rhPPCA + CPH | M/F | *PPCA*$^{-/-}$ | 0.2 | 24 |
| 5 | rhPPCA + CPH | M/F | *PPCA*$^{-/-}$ | 0.6 | 24 |
| 6 | rhPPCA + CPH | M/F | *PPCA*$^{-/-}$ | 2.0 | 24 |
| 7 | rhPPCA + CPH | M/F | *PPCA*$^{-/-}$ | 6.0 | 24 |
| 8 | rhPPCA + CPH | M/F | *PPCA*$^{-/-}$ | 20.0 | 24 |
| 9 (recovery) | rhPPCA + CPH | M/F | *PPCA*$^{-/-}$ | 20.0 | 1 week |

[a]n = 10 mice per group, 5 males (M) and 5 females (F).
[b]Twice-weekly intravenous (i.v.) injections for 8 weeks.
[c]Time (hours) postinjection of final dose of rhPPCA.
[d]CPH (cyproheptadine) 10 mg/kg intraperitoneally (i.p.), 30 min prior to i.v. injection.

bone marrow were harvested from all animals and analyzed for cathepsin A, NEU1, and β-GAL activities, as well as β-HEX (hexosaminidase B) activity, used as a control enzyme not related to the three-enzyme complex. Compared to wild-type (WT) samples, the activities of cathepsin A and NEU1 were drastically reduced or undetectable in all tissues of untreated *PPCA*$^{-/-}$ mice, whereas those of β-GAL and β-HEX were significantly increased (Figures 3A–3P and S2A–S2L; Tables S4–S7). Following treatment with rhPPCA for 8 weeks, a dose-dependent increase in cathepsin A activity was measured in most of the organs analyzed (Figures 3A–3D and S2A–S2C; Table S4). The highest activities were detected in the liver, spleen, and heart of mice treated with a 20-mg/kg dose of enzyme (147%, 222%, and 84% of the WT activity, respectively) (Figures 3A–3C; Table S4). Less penetrable tissues, such as kidney and brain, still showed internalization of the recombinant enzyme but to a lesser extent (19% and 14% of WT, respectively) (Figures 3D and S2B; Table S4), albeit its therapeutic potential, at least in the brain, needs to be further investigated. In the recovery group (20 mg/kg; recovery), cathepsin A activity was still detectable, although to a lesser extent, in some tissues with the heart and spleen showing a modest increase in activity relative to untreated *PPCA*$^{-/-}$ mice (group 3) at 8 weeks (Figures 3A–3D and S2A–S2C; Table S4). These data indicate that rhPPCA may not persist in tissues longer than 1 week following dose completion. Similar to the results observed in GS fibroblasts, the increased cathepsin A activity in rhPPCA-injected mice was paralleled by an increase in NEU1 activity in most tissues tested (Figures 2E, 3E–3H, and S2D–S2F; Table S5). However, unlike the *in vitro* data performed in human GS fibroblasts (Figure 2F), treatment with rhPPCA, in *PPCA*$^{-/-}$ mice, led to normalization of β-GAL levels in almost all treatment groups, which correlated with similar reduction in β-HEX activity (Figures 3I–3P and S2G–S2L; Tables S6 and S7).

### *Histopathological analysis of tissues*

Immunohistochemistry with anti-hPPCA antibody confirmed the widespread distribution of rhPPCA in cells of various organs. Representative images of tissues from mice treated with 20 mg/kg rhPPCA (group 8) are shown in Figure 4A. Cytoplasmic vacuolation consisting of sparse fibrillar structures, reflecting lysosomal accumulation of low molecular weight compounds (e.g., oligosaccharides and/or glycopeptides), is one of the pathological hallmarks of GS.[4,26] To assess the reduction of lysosomal storage following treatment with rhPPCA, tissue sections were stained with hematoxylin and eosin (H&E) and scored based on the degree and severity of cytoplasmic vacuolation. Figure 4B shows representative histopathology images of the liver, kidney, heart, and spleen of mice treated with the 2-mg/kg dose that demonstrates overt correction of lysosomal vacuolation already at this low dose. The dot plots in Figures 5 and S3–S7 summarize the pathology scoring of all tissues, where each dot refers to a sample obtained from an individual animal. Scoring was performed by a certified veterinary pathologist blinded to treatment groups. Tissues from WT mice receiving only vehicle were included in group 1. Vehicle-treated *PPCA*$^{-/-}$ mice (group 3, knockout [KO] + CPH) had severe cytoplasmic vacuolation present in all tissues tested, as deduced from their high pathology scores (Figures 5 and S3–S7; Table S8). Lower, dose-dependent scores were assigned to the tissues of treated mice, such as kidney, brain, muscle, and lung, a finding that was in agreement with the corresponding levels of measured enzyme activities (Figures 5A–5C and S3; Tables S4, S5, and S8). At a cellular level, liver Kupffer cells, spleen macrophages, and bone osteoclasts were easily cleared of storage even at the 0.2- and 0.6-mg/kg doses, whereas heart macrophages were cleared at the 2-mg/kg dose (Figures 5D–5H and S4; Table S8). At 20 mg/kg rhPPCA, the cytoplasmic vacuolation was no longer evident in tissues from all systemic organs (Figures 5 and S3–S7; Table S8). However, in the brain, only the choroid plexus responded to the treatment, whereas neurons and glia did not show signs of reduced storage, even in mice treated with the highest dose of enzyme (Figures S3A–S3C; Table S8). The ganglion cells and tissue macrophages in the small intestine remained severely vacuolated but were cleared at 20 mg/kg rhPPCA (Figures S5A and S5B; Table S8). Selected tissues, such as follicular epithelium and C cells in the thyroid; tissue macrophages in the thymus and eye; podocytes in the kidney; epithelium in the epididymis; interstitial cells, stromal capsule cells, and germinal epithelium in the testis; and endometrial stromal cells of the uterus and the tissue macrophages in the uterus and ovary did not demonstrate reversal of the phenotype until doses of $\geq$6 mg/kg rhPPCA (Figures 5C and S6; Table S8). Interestingly, a significant reduction in the extent of muscle degeneration and fibrosis was noted in *PPCA*$^{-/-}$ mice receiving as low as $\geq$2 mg/kg rhPPCA (Figures S3D and S3E; Table

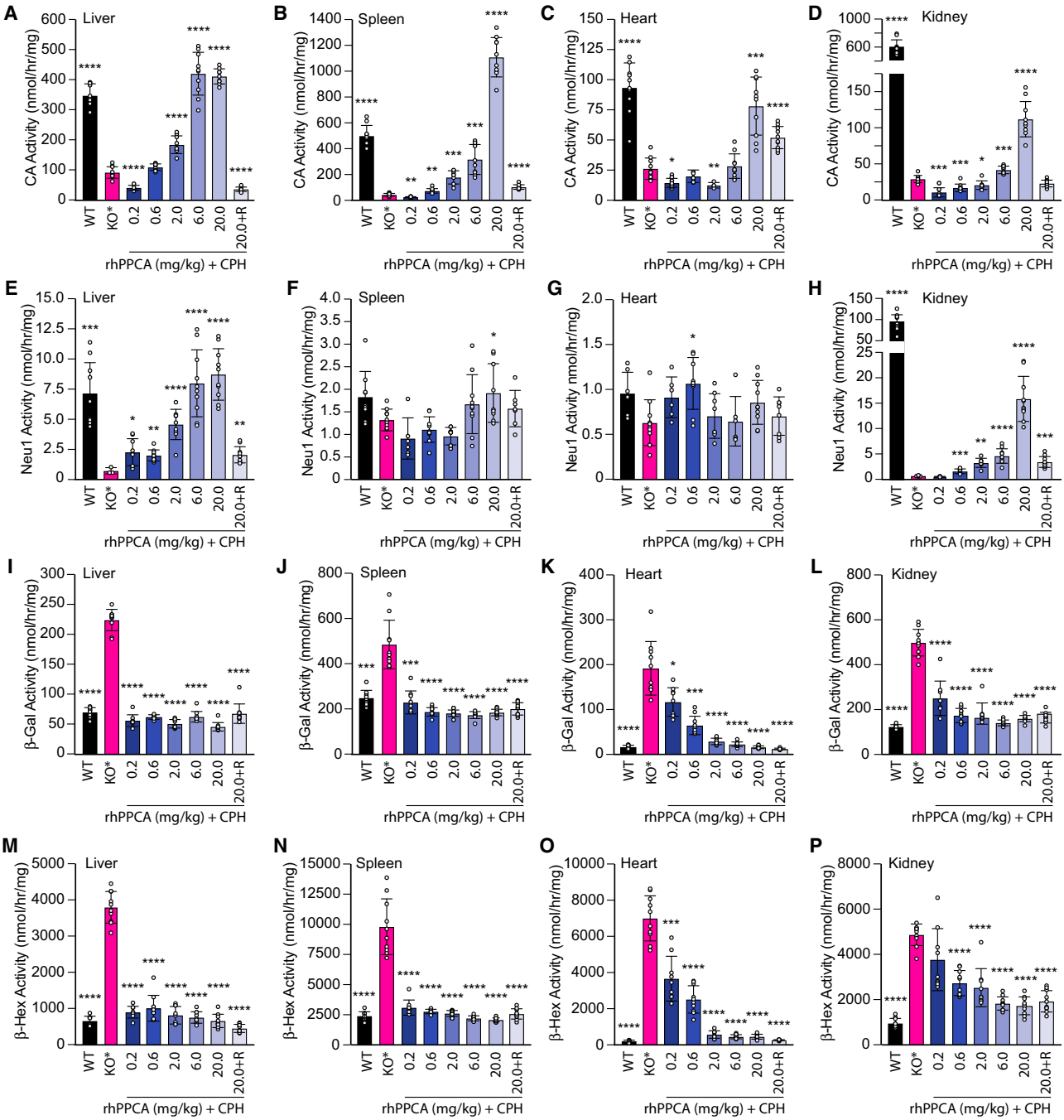


**Figure 3. rhPPCA restores cathepsin A activity and corrects NEU1 and β-GAL activities in *PPCA*$^{-/-}$ mice**

(A–D) Cathepsin A (CA) activity measured in liver, spleen, heart, and kidney lysates from *PPCA*$^{-/-}$ mice treated with rhPPCA (doses: 0.2, 0.6, 2.0, 6.0, and 20 mg/kg, corresponding to groups 4, 5, 6, 7, and 8, respectively) for 8 weeks from untreated wild-type (WT) FVB/NJ mice (group 1) and from untreated *PPCA*$^{-/-}$ (KO) mice (group 3). Group 9, designated 20.0 + R, represents the recovery group sacrificed 1 week after the final injection, n ≥ 4. (E–P) NEU1 (E–H), β-GAL (I–L), and β-HEX (M–P) activities measured in the same set of tissues as above, n ≥ 3. KO*, *PPCA*$^{-/-}$ + CPH. All of the graphs are presented as mean ± SD. Statistical analyses were performed using the Brown-Forsythe and Welch ANOVA tests. *p < 0.05, **p < 0.01, ***p < 0.001, ****p < 0.0001.

S8). A reduction in severity or incidence of the arthritis and degeneration and necrosis of the articular cartilage within the stifle joint and/or growth plate cartilage were noted in *PPCA*$^{-/-}$ mice receiving ≥6 mg/kg rhPPCA (Figure S7; Table S8). A similar reduction in cytoplasmic vacuolation was also observed in the recovery group (20 mg/kg; recovery) compared to group 8 (20 mg/kg) (Figures 5

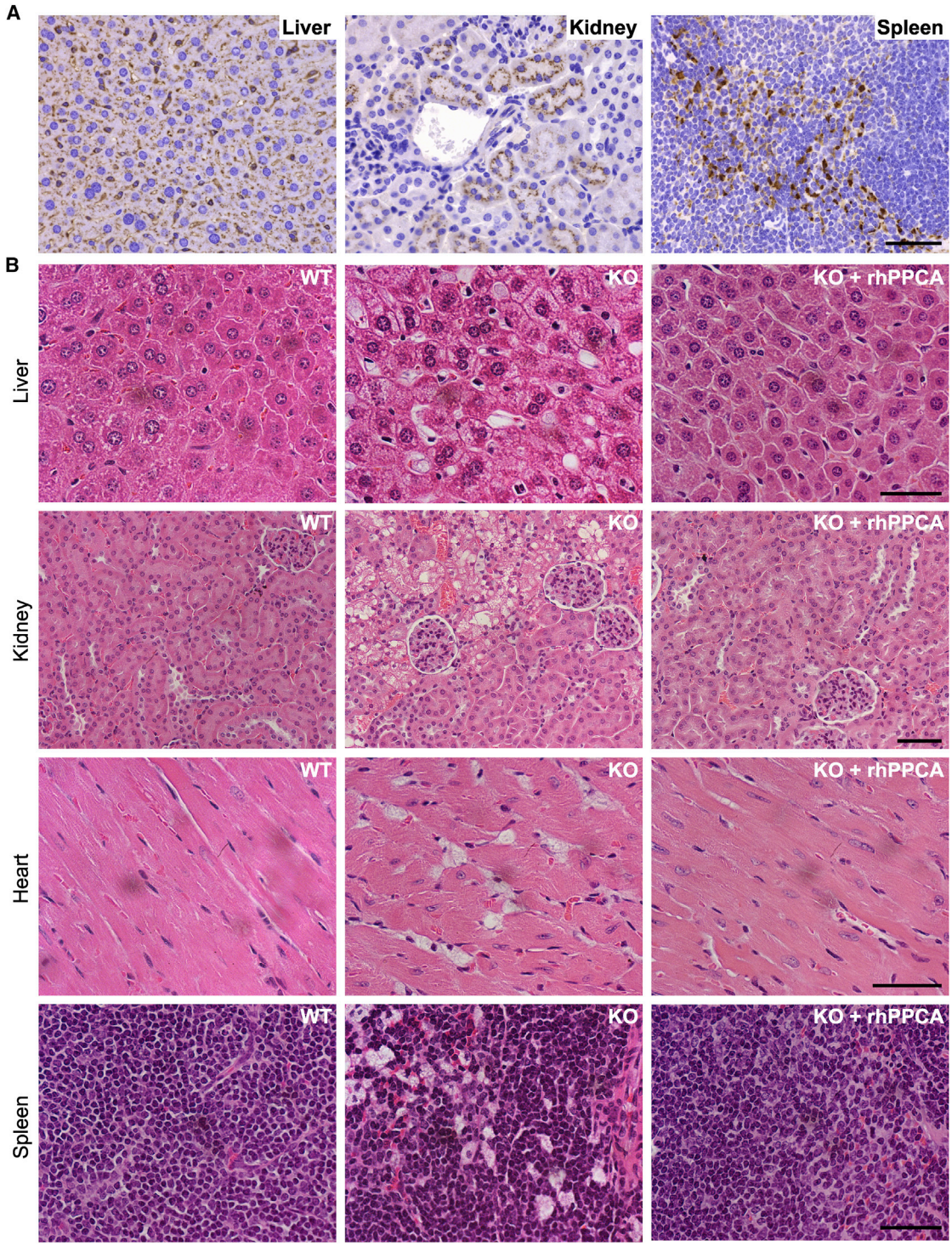


**Figure 4. rhPPCA is taken up by cells of *PPCA*$^{-/-}$ visceral organs and reduces lysosomal vacuolation**

(A) Representative immunohistochemistry images of liver, kidney, and spleen from mice treated with 20 mg/kg rhPPCA (group 8) showing widespread distribution of rhPPCA. Scale bar, 50 μm. (B) Representative histopathology images of the liver, kidney, heart, and spleen of untreated WT and *PPCA*$^{-/-}$ (KO) mice and of *PPCA*$^{-/-}$ (KO) mice treated with 2 mg/kg rhPPCA (groups 1, 3, and 6, respectively). Scale bars, 50 μm, 100 μm, 50 μm, and 50 μm, respectively.

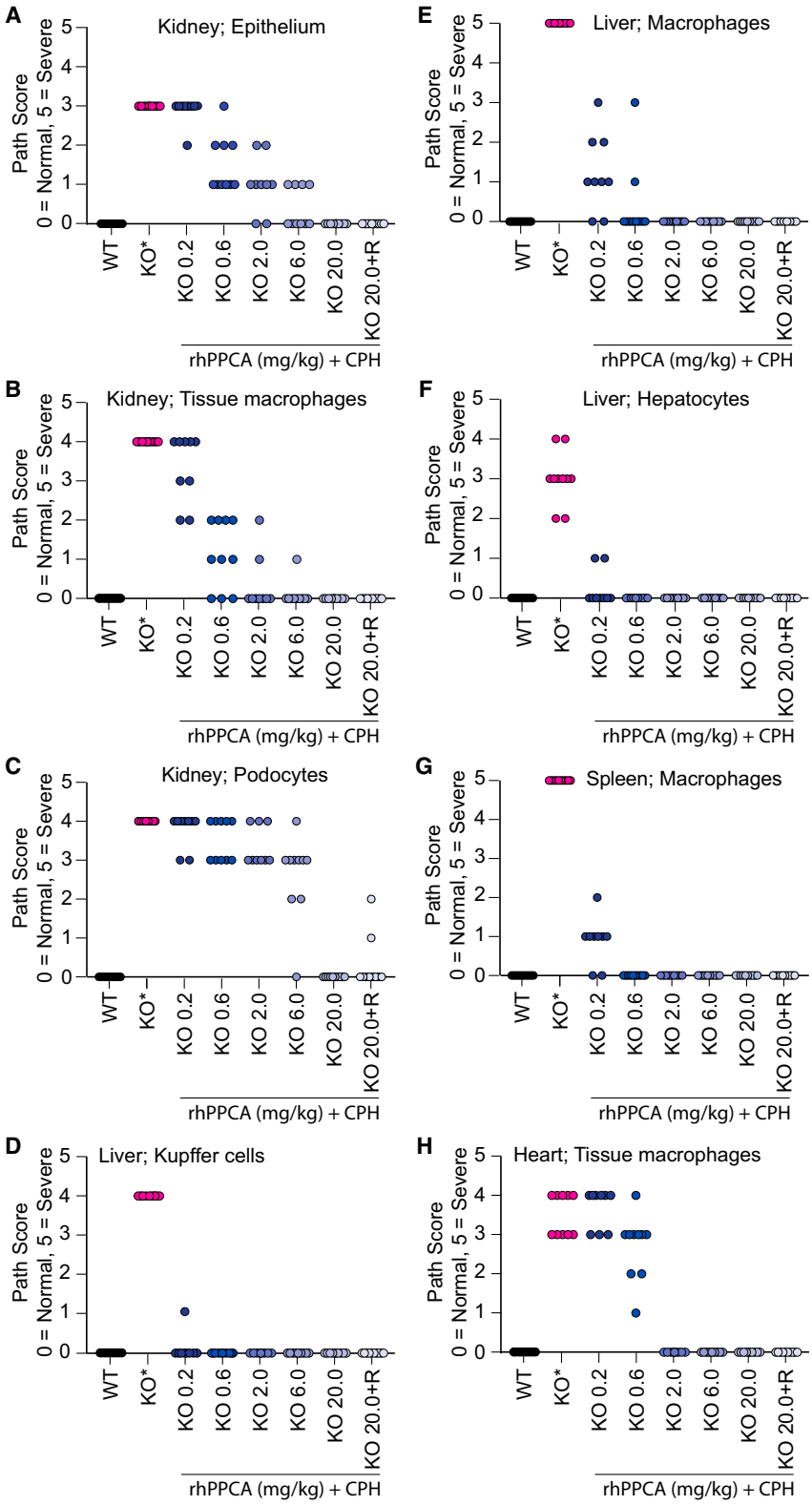


**Figure 5. Quantification of lysosomal vacuolation in *PPCA*$^{-/-}$ mice after treatment with rhPPCA**

(A–H) Histopathological analyses of kidney (A–C), liver (D–F), spleen (G), and heart (H). Correction of tissue morphology after rhPPCA treatment of *PPCA*$^{-/-}$ mice was quantified based on the extent of lysosomal vacuolation in cells of these organs. Mean path score of individual mice was graded: 1, minimal; 2, mild; 3, moderate; 4, marked; and 5, severe. Scores obtained from mice treated with rhPPCA (doses: 0.2, 0.6, 2.0, 6.0, and 20 mg/kg, corresponding to groups 4, 5, 6, 7, and 8, respectively) for 8 weeks were plotted with scores from WT FVB/NJ mice (group 1) and from untreated *PPCA*$^{-/-}$ (KO) mice (group 3). Group 9, designated 20.0 + R, represents the recovery group sacrificed 1 week after the final injection. Each dot represents an individual mouse in the study, $n \geq 9$.

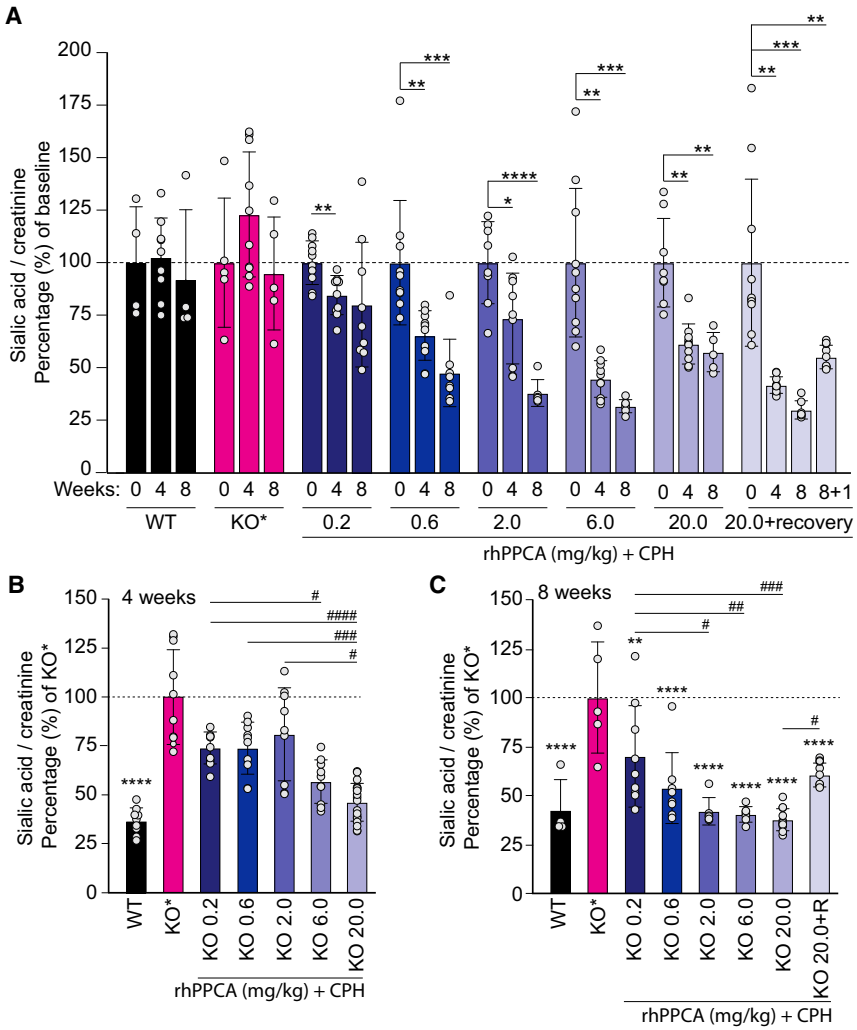


**Figure 6. rhPPCA reduces urinary sialylated oligosaccharides in *PPCA*$^{-/-}$ mice in a dose-dependent manner**

(A) Urinary sialic acid after 4 (mid-study), 8 (end of study), and 8 + 1 (group 9, 20.0 + recovery) weeks of treatment with rhPPCA was compared to the levels measured at week 0, used as baseline. (B and C) Sialic acid levels were compared among doses (0.2, 0.6, 2.0, 6.0, and 20 mg/kg) at 4 (B) and 8 and 8 + 1 (recovery group) (C) weeks, respectively. KO*, group 3, *PPCA*$^{-/-}$ (KO) + CPH. Urinary sialic acid levels were normalized to a creatinine concentration; data are presented as mean ± SD. The dots in the graphical bars represent values obtained from each single mouse. Statistical analyses were performed using the Brown-Forsythe and Welch ANOVA tests, n ≥ 4. *p < 0.05, **p < 0.01, ***p < 0.001, ****p < 0.0001; #p < 0.05, ##p < 0.01, ###p < 0.001, ####p < 0.0001. The asterisk (*) is used to label groups compared to KO* = group 3; #, used to label comparisons among groups treated with different doses of rhPPCA.

and S3–S7; Table S8), where clearance was still maintained 1 week after dose cessation. Although the levels of cathepsin A and NEU1 activities were diminished in most tissues in the recovery group (20 mg/kg; recovery), sustained reduction in cytoplasmic vacuolation demonstrates the durability of treatment beyond the tissue PKs of rhPPCA (Figures 3, 5, and S2–S7; Tables S4, S5, and S8). This could be due to the increase in stability of lysosomal rhPPCA when bound to NEU1 and β-GAL.

### *Dose-dependent reduction of urinary sialylated oligosaccharides upon treatment with rhPPCA*

Progressive accumulation of sialylated oligosaccharides in tissues, serum, and urine due to loss of a functional PPCA-NEU1-β-GAL complex is a diagnostic hallmark of GS patients.[4] To assess the effect of rhPPCA on the clearance of sialylated oligosaccharides in bodily fluids, urinary sialic acids were measured using an enzymatic assay. All measurements were normalized to creatinine concentration and plotted as a percent change from baseline at a post-4-week dose (halfway through the study), at a post-8-week dose (end of study), and at a post-8 week dose followed by 1 week recovery (Figure 6). After treatment with rhPPCA, there was a rapid decrease in sialic acid levels, with greater changes observed at higher doses of rhPPCA >0.6 mg/kg (Figure 6A). The recovery group, which received treatment for 8 weeks at 20 mg/kg, followed by 1 week of no dose prior to euthanization (group 9), showed decreasing levels of total sialic acid in urine at 8 weeks ; however, the 1-week recovery period showed partial reaccumulation of substrate, indicating the need for a continued dosing regimen (Figure 6A). A dose-dependent decrease of urinary sialic acid was observed at doses >6 mg/kg in the 4-week group but was already apparent at 0.6 mg/kg in the 8-week group (Figures 6B and 6C).

## DISCUSSION

The complex and diverse clinical phenotypes characteristic of lysosomal storage diseases (LSDs) represent a serious challenge for the development of adequate and effective treatments for patients affected by these conditions.[27] This challenge is aggravated by the fact that most LSDs have neurological manifestations, often associated with mental retardation, that are difficult or impossible to treat due to the inability of the therapeutic product to cross the blood-brain barrier.[28] However, for some LSDs, clinical trials are currently ongoing, and patients are being treated by administering the missing enzyme exogenously via ERT, by diminishing the amount of storage products with substrate reduction therapy, or by enhancing residual enzyme activity by chaperones that aid in the folding and stability of the mutant enzymes.[27]

So far, one of the preferred therapeutic approaches for LSDs linked to single enzyme deficiency has been ERT, and diseases, such as

Gaucher; Fabry; Pompe; and MPS I (Mucopolysaccharidosis type I), MPS VI, MPS IVA, and MPS VII, have been treated with this method for many years.[27,29–34] Additional therapeutic strategies have also been implemented in LSD patients, including hematopoietic stem cell transplantation and *in vivo* or *ex vivo* gene therapy, each of them carrying intrinsic limitations and benefits.[27,35–38] Foremost, the biochemical properties of the therapeutic enzyme and the nature of the storage products and their biodistribution in different tissues and organs are some of the factors that need to be taken into account in designing tailored therapies for LSDs. Thus, a better understanding of disease pathogenesis and the ability to test various therapeutic interventions in suitable models of these diseases may instruct us on the potential hurdles that need to be circumvented or addressed before moving any therapy into a clinical setting.

In this respect, the $PPCA^{-/-}$ mice have served as a powerful *in vivo* model for testing investigational therapies for GS, as a prelude to the preclinical studies described here. Transplantation of $PPCA^{-/-}$ mice with transgenic bone marrow overexpressing a human PPCA mini gene exclusively in erythroid precursors or monocytes/macrophages afforded a significant or complete reversal of the disease phenotype in the systemic organs and partial correction of the brain pathology, including reduced loss of Purkinje cells.[14,16] More recently, a preclinical dose-finding, gene-therapy study was conducted in the same mouse model, using a recombinant AAV vector in which human PPCA was expressed under the control of a liver-specific promoter.[17] Prolonged overexpression of the enzyme in the liver of treated mice resulted in sustained release of the PPCA precursor in circulation, its internalization by cells of all visceral and reproductive organs, complete correction of the histopathology, and rescue of male and female fertility. Overall, these studies have set the basis for the development of a therapeutic product that could be used in the clinic for the treatment of GS patients. The biochemical features of PPCA, including its relatively long half-life in tissues and the fact that the precursor is secreted as a zymogen and is internalized by multiple recipient cells,[15] make this enzyme particularly suitable for ERT.

In the current proof-of-concept study, we demonstrate that a rhPPCA precursor produced in CHO cells and purified to homogeneity from the culture medium is efficiently taken up by deficient cells, routed to the lysosomes, and converted into its mature and active form. Restoration of cathepsin A activity is accompanied by normalization of the activities of NEU1 and β-GAL, both in human patient-derived GS fibroblasts, as well as in the GS mouse model. Particularly relevant is the observed increase in cathepsin A activity in difficult-to-treat organs, such as the kidney and the heart. These results are noteworthy in view of the fact that children affected by GS, including those with the non-neuropathic, attenuated form of the disease, develop severe nephropathy and cardiac problems that could be fatal as the patient ages.[3,4] We also found an increase in cathepsin A activity in the brain of mice treated with the high dose of the recombinant enzyme. This could be due to the inherent brain inflammation associated with the disease that may trigger the recruitment of PPCA-positive, blood-derived monocytes/microglia, leading to correction of their functional activity in the brain, as previously observed in GM1 gangliosidosis and other LSD mouse models post-treatment.[39] Alternatively, it is still conceivable that small amounts of circulating proteins administered intravenously could cross the blood-brain barrier by transcytosis, as proposed to occur in other LSDs and disease mouse models.[27,40,41] Generally, however, ERT is not likely to be effective for correcting the disease in the nervous system, unless the recombinant enzyme is directly routed into the CNS via intrathecal, intracisternal, or intraventricular injection,[42,43] taking into account the caveats associated with this approach. Thus, as of today, ERT is still the least invasive, albeit costly, approach for the treatment of the non-neuropathic forms of LSDs, including GS.

Patients with the late infantile form of GS comprise a unique group because most of the confirmed diagnosed patients share at least one of two allelic *PPCA* mutations, and they show no or only minor cognitive impairment.[4] Although the reported cases of late infantile GS are just a few, it is becoming increasingly clear that particularly milder cases of LSDs are often not recognized or misdiagnosed.[44,45] There are, in fact, patients that present with no clinical and biochemical features characteristic of the disease, such as oligosacchariduria, and have been diagnosed only by whole exome sequencing.[44] Thus, GS may fall into the category of orphan diseases that are, in fact, more frequent than expected; in this case, the number of patients eligible for therapy could be greater than anticipated. In addition, there is now evidence that the activity of mutant NEU1 in the attenuated type I forms of sialidosis,[46] as well as in animal models mimicking type I sialidosis,[47] can be increased by exogenously incrementing PPCA levels. It is therefore conceivable that a rhPPCA therapeutic product could be used to treat both non-neuropathic GS and sialidosis patients.

In conclusion, with the consideration that we have not observed any toxicity nor adverse clinical signs associated with the administration of rhPPCA at doses $\geq$ 20 mg/kg over a period of 8 weeks, we can foresee that this therapeutic product may be effective and safe and that rhPPCA-mediated ERT has the potential to be translated to the clinic for the treatment of non-neuropathic GS patients.

## MATERIALS AND METHODS

### Animal models

Animals were housed in a fully AAALAC (Assessment and Accreditation of Laboratory Animal Care)-accredited animal facility with controlled temperature (22°C), humidity, and lighting (alternating 12 h light/dark cycles). Food and water were provided *ad libitum*. All procedures in mice were performed according to animal protocols approved by the St. Jude Children's Research Hospital Institutional Animal Care and Use Committee (IACUC) and NIH guidelines. $PPCA^{-/-}$ and *WT* mice were bred into the FVB/NJ genetic background. Animals (WT, not injected, and injected mice) were sacrificed at 12 weeks of age. The recovery group was sacrificed at 13 weeks, 1 week post-treatment.

### Production and purification of rhPPCA

cDNA for human PPCA subcloned into a eukaryotic expression vector pFN10A(ACT) Flexi vector (Promega, Madison, WI, USA)

containing the neomycin resistance marker was transfected into proprietary CHO cells. With the use of the neomycin-resistant proprietary CHO host cells, a CHO-hPPCA cell line was generated using a blasticidin-resistant gene. Neomycin- and blasticidin-resistant, stably transformed cell lines expressing hPPCA were isolated and grown in a chemically defined media.[19] The highest expression cone was expanded and adapted to suspension cultures in production medium. Bioreactor harvest was depth filtered and purified using a downstream purification process that included a combination of ion-exchange and hydrophobic chromatography steps. The final purified material was concentrated via an ultrafiltration/diafiltration step into the appropriate formulation buffer.

#### Determination of sialic acid on rhPPCA

The sialic acid content on the rhPPCA sample was determined by the 1,2-diamino-4,5-methylenedioxybenzene dihydrochloride (DMB) labeling method. PPCA sample was concentrated to ~1 mg/mL, and the sialic acid content on the protein (in triplicate) was chemically cleaved by the use of a dilute solution of hydrochloric acid and labeled with the substrate-specific fluorophore, DMB (Sigma, St. Louis, MO, USA). The samples were quenched with HPLC-grade water and analyzed via a reverse-phase chromatography HPLC system equipped with fluorescence detection. The total sialic acid content on PPCA was determined from a standard curve generated using an appropriate standard (N-acetylneuraminic acid; Sigma, St. Louis, MO, USA).

#### Determination of M6P content on rhPPCA

This method utilized release of M6P residues from rhPPCA by acid hydrolysis using trifluoroacetic acid (TFA) at 100°C for 90 min. The hydrolyzed samples were labeled with 4-aminobenzoic acid ethyl ester (4-ABEE) via reductive amination. Labeled samples and standards were then analyzed via reverse-phase HPLC equipped with fluorescence detection on a Phenomenex Luna C18 column (5 μm, 100 Å, 4.6 × 250 mm), which separates molecules based on hydrophobicity. A fluorescence detector was used to measure the M6P-ABEE analyte with an excitation of 305 nm and emission wavelength of 360 nm. The total M6P content was then quantitated against the M6P standard curve.

#### PKs of rhPPCA in male Sprague-Dawley rats

The PKs of rhPPCA in serum and tissues of Sprague-Dawley rats were measured after a single-dose intravenous injection of rhPPCA or vehicle (PBS). Serial blood samples were collected at pre-dose at 2, 5, 10, 15, 30, and 60 min and at 2 h postdose, whereas tissues were collected at 2, 6, 12, 24, 36, and 48 h postinjection. PK variables were estimated by noncompartmental analysis using WinNonlin Enterprise (version [v.]6.2) software. Nominal sample times were used for determination of the PK parameters. The $C_{max}$ and $T_{max}$ were derived directly from the serum concentration-time profiles.

#### $K_{uptake}$ determination of rhPPCA in GS fibroblasts

GS fibroblasts were passaged from a confluent, 150-mm flask into two, 24-well culture dishes at 100,000 cells/well, 48 h before uptake experiments. An 11-point dose-response curve of rhPPCA was prepared in growth media ranging from 15 nM to 0.26 nM final concentration of rhPPCA per well and was administered to cells in quadruplicate sets. An untreated control was included in each set. To determine competitive uptake, one set was coincubated with 5 mM M6P (Sigma, St. Louis, MO, USA) final concentration per well. Cells were treated with rhPPCA and rhPPCA + M6P for overnight uptake not exceeding 24 h. Cells were harvested by trypsinization, and a crude lysate was prepared by resuspending the pellets in water for lysis by hypotonic shock, as described previously. Cell lysates were assayed for cathepsin A activity and normalized to total protein concentration by BCA. Mean activity was plotted to generate dose-response curves using Softmax Pro software (Molecular Devices, Sunnyvale, CA, USA) by standard nonlinear regression analysis. Final calculation of $K_{uptake}$ was determined with Michaelis-Menten kinetics, Hanes-Woolf linear regression analysis.

#### *In vitro* uptake of rhPPCA in GS patient-derived fibroblasts

The GS human fibroblast line GM 21262 (Coriell Institute, Camden, NJ, USA) was maintained in 5% $CO_2$ at 37°C in MEM (Minimum Essential Media) supplemented with 10% fetal bovine serum (FBS), L-glutamine, and penicillin/streptomycin. Fibroblasts were passaged from a confluent, 150-mm flask into 24-well culture dishes at 100,000 cells/well, 48 h before uptake experiments. 1 μg purified rhPPCA was diluted in 1 mL growth medium per well. The cells were incubated in 5% $CO_2$ at 37°C for predetermined timed intervals not exceeding 24 h. Cells were harvested by trypsinization, and a crude lysate was prepared by resuspending the pellets in water for lysis by hypotonic shock for 30 min on ice. Cell lysates were assayed for cathepsin A, NEU1, and β-GAL activity, as described in the section below.

#### SDS-PAGE and immunoblotting

Purified rhPPCA was diluted 1:1 with 2× SDS sample buffer, with or without reducing agent, and heated to 95°C prior to loading. Purified protein was resolved in 12% Tris-glycine gels and visualized by staining with Coomassie brilliant blue. For western blot analysis, cell pellets were lysed in distilled water for lysis by hypotonic shock for 30 min on ice. Crude lysates were analyzed by BCA (Thermo Fisher Scientific, Waltham, MA, USA) and loaded based on total protein concentration. Samples were prepared 1:1 with 2× SDS sample buffer with 2-mercaptoethanol as the reducing agent and heated to 95°C prior to loading. Samples were run on 12% Tris-glycine gels, blotted onto polyvinylidene fluoride (PVDF) membranes, and probed with an anti-hPPCA polyclonal antibody (R&D Systems, Minneapolis, MN, USA) for overnight incubation. Membrane was incubated for 2 h with a donkey anti-goat immunoglobulin G (IgG) horseradish peroxidase (HRP; Santa Cruz Biotechnology, Santa Cruz, CA, USA) as a secondary antibody, developed using a chemiluminescent substrate, and imaged using the ChemiDoc Imager (Bio-Rad, Hercules, CA, USA).

#### Tissue processing and homogenization

Frozen tissues were briefly thawed and weighed to determine the adequate extraction volume. In general, to 50 mg−100 mg pieces of

tissue, 10 vol of ice-cold ultrapure water without protease inhibitors was added. Homogenization was performed using a Polytron homogenizer (Kinematica, Switzerland) for 30 s at maximum speed until extracts appeared homogeneous. The blades were washed between each tissue and rinsed twice in water and once in 70% ethanol. For pieces of tissue weighing less than 50 mg, a minimum of 0.5 mL of extraction volume was added, using a Duall ground glass homogenizer for homogenization.

#### Enzyme activities (cathepsin A, NEU1, β-GAL, and β-HEX)

Four enzymatic assays were performed in parallel: cathepsin A, NEU1, β-GAL, and β-HEX activities. Crude extracts were prepared as described in the tissue-processing and homogenization section, kept on ice, and diluted in an enzyme dilution buffer (EDB; 50 mM sodium acetate, pH 5.0/100 mM NaCl/1 mg/mL bovine serum albumin [BSA; w/v]/0.02% sodium azide [w/v]). Crude extracts were incubated with fluorogenic peptide substrates specific for each enzyme measured: N-carbobenzoxy-L-phenylalanyl-L-alanine (Z-Phe-Ala) (Sigma, St. Louis, MO, USA) for cathepsin A activity (without substrate: 50 mM 2-[N-morpholino]ethane sulfonic acid [MES], pH 5.5, or with substrate: 50 mM MES, pH 5.5, + 1.5 mM Z-Phe-Ala); 2′-(4-methylumbelliferyl)-α-D-N-acetylneuraminic acid (Sigma, St. Louis, MO, USA) for NEU1 activity (0.5 M Na-acetate, pH 4.3); 4-methylumbelliferyl β-D-galactopyranoside (Sigma, St. Louis, MO, USA) for β-GAL activity (0.1 M Na-acetate, pH 4.3); and 4-methylumbelliferyl N-acetyl-β-D-glucosaminide (Sigma, St. Louis, MO, USA) for β-HEX activity (3 mM in citrate-phosphate buffer, pH 4.4). The reactions were incubated at 37°C in the pH-dependent buffers specific for each enzyme ( cathepsin A , pH 5.5; NEU1, pH 4.3; β-GAL, pH 4.3; β-HEX, pH 4.4) for 1 h. The reaction was stopped with 200 μL carbonate stop buffer (0.5 M $Na_2CO_3$ with the pH set to 10.7 by adding 0.5 M $NaHCO_3$) for NEU1, β-GAL, and β-HEX activities. Cathepsin A activity was stopped at 100°C for 5 min, and 10 μL reaction mix was read in 250 μL, 50 mM Na-carbonate stop buffer (pH 9.5) containing 500 μL o-phthaldialdehyde (10 mg/mL), and 500 μL 2-mercaptoethanol (5 μL/1mL 100% ethanol). The amount of fluorescence generated from each reaction indicates cleavage of the fluorescent tag from its peptide substrate and is proportional to the amount of enzyme present. The mean fluorescence of samples given assay buffer was subtracted from the mean fluorescence of samples given assay buffer plus the specific substrate. Mean fluorescence values were interpolated to a standard curve, adjusted for dilution and length of incubation, and normalized to protein by BCA. The final units of activity were reported as nanomoles per hour per milligram.

#### H&E histopathology

Tissues were fixed in 10% neutral-buffered formalin for 48 h at room temperature and stored in 70% ethanol. All samples were processed, sectioned, and embedded onto slides for staining with H&E. Light microscopy evaluation was conducted by a board-certified veterinary pathologist blinded to the study. The tissues were scored for the presence of lysosomal storage, as determined by the extent of vacuolation of cells, as well as overall cell morphology. The severity of lysosomal storage, as indicated by cytoplasmic vacuolation, is summarized by a mean path score in each tissue element using the following key: 1 = minimal; 2 = mild; 3 = moderate; 4 = marked; 5 = severe. Additionally, the tissues were evaluated for toxicological effects of rhPPCA.

#### Immunohistochemistry

6 μm-thick paraffin-embedded tissue sections were subjected to deparaffinization and antigen retrieval using standard histology methods. After blocking with 0.1% BSA and 0.5% Tween 20, the sections were incubated overnight at room temperature with anti-PPCA antibody. The sections were washed and incubated with biotinylated secondary goat anti-rabbit antibody (Jackson ImmunoResearch Laboratories, West Grove, PA, USA) for 1 h. Endogenous peroxidase was removed by incubating the sections with 0.1% hydrogen peroxidase for 30 min. Antibody detection was performed using the ABC Kit and diaminobenzidine substrate (Vector Laboratories, Burlingame, CA, USA), and sections were counterstained with hematoxylin, according to the standard method.

#### Enzychrome sialic acid assay for total urine sialyloligosaccharides

The sialyloligosaccharide content in mouse urine was determined by the release of bound sialic acid using an Enzychrome Sialic Acid Assay Kit from BioAssay Systems (ESLA-100; Hayward, CA, USA). Urine was collected from individual animals at a baseline time point (24 h prior to treatment), half-way through the study at 4 weeks (24 h post the last dose), and at necropsy. Urine samples were initially diluted in PBS, and total sialic acid (free and bound) was measured following acid hydrolysis for 1 h at 80°C. After the addition of neutralization buffer, samples were set to cool at room temperature and diluted further in an enzymatic master mix, which utilizes an enzyme-coupled reaction to oxidize any liberated sialic acid. A standard curve was generated from a 10-mM sialic acid stock solution that was serially diluted in ultra-pure water. The curve was plotted as a function of fluorescence and analyzed by a linear curve fit using a template created in the SoftMax Pro software v.6.5 (Molecular Devices, Sunnyvale, CA, USA). All unknown samples were interpolated to the standard curve to yield a concentration value in nanomolar Sialic Acid. Final sialic acid concentrations were normalized to creatinine and expressed as microgram sialic acid/microgram creatinine.

#### Creatinine concentration in urine

The creatinine concentration in urine samples was determined by a procedure based on Jaffe's reaction, where creatinine and picric acid under alkaline conditions yield a quantitative colorimetric reaction. Urine samples were diluted 1:8 with ultrapure water. 80 μL diluted samples were transferred to a 96-well assay plate. A working solution containing 3 mL of 1% picric acid and 3 mL of 0.75 N NaOH were mixed together in which 40 μL of working reagent was added to all wells. The samples were incubated at room temperature for 15 min to allow for adequate color development in which its absorbance was measured at 520 nm. A standard curve was generated from a purified creatinine stock solution, which was serially diluted in ultrapure water. Absorbance values were plotted and analyzed by a linear curve fit using a template created in the SoftMax Pro software v.6.5 (Molecular

Devices, Sunnyvale, CA, USA). All unknown samples were interpolated to the standard curve to yield a final creatinine concentration expressed in micrograms per milliliter.

### Statistical analysis

Statistical analyses were performed with an ordinary one-way ANOVA (multiple comparisons) or the Brown-Forsythe and Welch ANOVA test (multiple comparisons) using GraphPad Prism. The data are presented as mean or average ± SD. The values of $p < 0.05$ were considered statistically significant.

## SUPPLEMENTAL INFORMATION

Supplemental Information can be found online at https://doi.org/10.1016/j.omtm.2020.11.012.

## ACKNOWLEDGMENTS

We thank Maggie Wright (Ultragenyx Pharmaceuticals) for some of the tissue histopathology images and Peter Mutch (ICON) for consulting services regarding the PK analysis. We would also like to acknowledge Dr. James T. Raymond (Charles River, Frederick, MD, USA) for his help with the histopathology data and images. A.d.A. holds the Jewelers for Children Endowed Chair in Genetics and Gene Therapy. This work was funded by NIH grants GM104981 and DK095169, Ultragenyx Pharmaceuticals, The Assisi Foundation of Memphis, and the American Lebanese Syrian Associated Charities (ALSAC).

## AUTHOR CONTRIBUTIONS

Conceptualization, E.K., M.V., and A.d.A.; Methodology, J.C., H.H., E.G., R.M., G.B., K.J., B.G., M.M., and V.K.; Investigation, A.d.A., V.K., M.V., and G.B.; Production of Recombinant hPPCA, S.C. and V.K.; Writing – Original Draft, J.C. and V.K.; Writing – Review & Editing, A.d.A., I.A., and D.v.d.V.; Funding Acquisition, E.K., M.V., and A.d.A.; Supervision, A.d.A., G.B., and V.K.

## DECLARATION OF INTERESTS

The authors declare no competing interests.

## REFERENCES

1. D'Azzo, A., Hoogeveen, A., Reuser, A.J., Robinson, D., and Galjaard, H. (1982). Molecular defect in combined beta-galactosidase and neuraminidase deficiency in man. Proc. Natl. Acad. Sci. USA *79*, 4535–4539.

2. Bonten, E.J., Annunziata, I., and d'Azzo, A. (2014). Lysosomal multienzyme complex: pros and cons of working together. Cell. Mol. Life Sci. *71*, 2017–2032.

3. Annunziata, I., and d'Azzo, A. (2017). Galactosialidosis: historic aspects and overview of investigated and emerging treatment options. Expert Opin. Orphan Drugs *5*, 131–141.

4. d'Azzo, A., Andria, G., Bonten, E., and Annunziata, I. (2014). Galactosialidosis. The Online Metabolic and Molecular Bases of Inherited Disease*Volume 183* (McGraw-Hill Medical).

5. Galjart, N.J., Gillemans, N., Harris, A., van der Horst, G.T., Verheijen, F.W., Galjaard, H., and d'Azzo, A. (1988). Expression of cDNA encoding the human "protective protein" associated with lysosomal beta-galactosidase and neuraminidase: homology to yeast proteases. Cell *54*, 755–764.

6. Galjart, N.J., Morreau, H., Willemsen, R., Gillemans, N., Bonten, E.J., and d'Azzo, A. (1991). Human lysosomal protective protein has cathepsin A-like activity distinct from its protective function. J. Biol. Chem. *266*, 14754–14762.

7. Jackman, H.L., Morris, P.W., Deddish, P.A., Skidgel, R.A., and Erdös, E.G. (1992). Inactivation of endothelin I by deamidase (lysosomal protective protein). J. Biol. Chem. *267*, 2872–2875.

8. Jackman, H.L., Tan, F.L., Tamei, H., Beurling-Harbury, C., Li, X.Y., Skidgel, R.A., and Erdös, E.G. (1990). A peptidase in human platelets that deamidates tachykinins. Probable identity with the lysosomal "protective protein". J. Biol. Chem. *265*, 11265–11272.

9. Seyrantepe, V., Hinek, A., Peng, J., Fedjaev, M., Ernest, S., Kadota, Y., Canuel, M., Itoh, K., Morales, C.R., Lavoie, J., et al. (2008). Enzymatic activity of lysosomal carboxypeptidase (cathepsin) A is required for proper elastic fiber formation and inactivation of endothelin-1. Circulation *117*, 1973–1981.

10. Bonten, E.J., Galjart, N.J., Willemsen, R., Usmany, M., Vlak, J.M., and d'Azzo, A. (1995). Lysosomal protective protein/cathepsin A. Role of the "linker" domain in catalytic activation. J. Biol. Chem. *270*, 26441–26445.

11. van der Spoel, A., Bonten, E., and d'Azzo, A. (1998). Transport of human lysosomal neuraminidase to mature lysosomes requires protective protein/cathepsin A. EMBO J. *17*, 1588–1597.

12. Bonten, E.J., and d'Azzo, A. (2000). Lysosomal neuraminidase. Catalytic activation in insect cells is controlled by the protective protein/cathepsin A. J. Biol. Chem. *275*, 37657–37663.

13. Caciotti, A., Catarzi, S., Tonin, R., Lugli, L., Perez, C.R., Michelakakis, H., Mavridou, I., Donati, M.A., Guerrini, R., d'Azzo, A., and Morrone, A. (2013). Galactosialidosis: review and analysis of CTSA gene mutations. Orphanet J. Rare Dis. *8*, 114.

14. Zhou, X.Y., Morreau, H., Rottier, R., Davis, D., Bonten, E., Gillemans, N., Wenger, D., Grosveld, F.G., Doherty, P., Suzuki, K., et al. (1995). Mouse model for the lysosomal disorder galactosialidosis and correction of the phenotype with overexpressing erythroid precursor cells. Genes Dev. *9*, 2623–2634.

15. Bonten, E.J., Wang, D., Toy, J.N., Mann, L., Mignardot, A., Yogalingam, G., and D'Azzo, A. (2004). Targeting macrophages with baculovirus-produced lysosomal enzymes: implications for enzyme replacement therapy of the glycoprotein storage disorder galactosialidosis. FASEB J. *18*, 971–973.

16. Hahn, C.N., del Pilar Martin, M., Zhou, X.Y., Mann, L.W., and d'Azzo, A. (1998). Correction of murine galactosialidosis by bone marrow-derived macrophages overexpressing human protective protein/cathepsin A under control of the colony-stimulating factor-1 receptor promoter. Proc. Natl. Acad. Sci. USA *95*, 14880–14885.

17. Hu, H., Gomero, E., Bonten, E., Gray, J.T., Allay, J., Wu, Y., Wu, J., Calabrese, C., Nienhuis, A., and d'Azzo, A. (2012). Preclinical dose-finding study with a liver-tropic, recombinant AAV-2/8 vector in the mouse model of galactosialidosis. Mol. Ther. *20*, 267–274.

18. Leimig, T., Mann, L., Martin, Mdel.P., Bonten, E., Persons, D., Knowles, J., Allay, J.A., Cunningham, J., Nienhuis, A.W., Smeyne, R., and d'Azzo, A. (2002). Functional amelioration of murine galactosialidosis by genetically modified bone marrow hematopoietic progenitor cells. Blood *99*, 3169–3178.

19. Sethuraman, N., and Stadheim, T.A. (2006). Challenges in therapeutic glycoprotein production. Curr. Opin. Biotechnol. *17*, 341–346.

20. Tian, W., Ye, Z., Wang, S., Schulz, M.A., Van Coillie, J., Sun, L., Chen, Y.H., Narimatsu, Y., Hansen, L., Kristensen, C., et al. (2019). The glycosylation design space for recombinant lysosomal replacement enzymes produced in CHO cells. Nat. Commun. *10*, 1785.

21. Kornfeld, S. (1990). Lysosomal enzyme targeting. Biochem. Soc. Trans. *18*, 367–374.

22. Kakkis, E.D., Matynia, A., Jonas, A.J., and Neufeld, E.F. (1994). Overexpression of the human lysosomal enzyme alpha-L-iduronidase in Chinese hamster ovary cells. Protein Expr. Purif. *5*, 225–232.

23. Rudenko, G., Bonten, E., d'Azzo, A., and Hol, W.G. (1995). Three-dimensional structure of the human 'protective protein': structure of the precursor form suggests a complex activation mechanism. Structure *3*, 1249–1259.

24. Kolli, N., and Garman, S.C. (2014). Proteolytic activation of human cathepsin A. J. Biol. Chem. *289*, 11592–11600.

25. Brooks, D.A. (1999). Immune response to enzyme replacement therapy in lysosomal storage disorder patients and animal models. Mol. Genet. Metab. *68*, 268–275.

26. van Pelt, J., Kamerling, J.P., Vliegenthart, J.F., Hoogeveen, A.T., and Galjaard, H. (1988). A comparative study of the accumulated sialic acid-containing oligosaccharides from cultured human galactosialidosis and sialidosis fibroblasts. Clin. Chim. Acta *174*, 325–335.

27. Platt, F.M., d'Azzo, A., Davidson, B.L., Neufeld, E.F., and Tifft, C.J. (2018). Lysosomal storage diseases. Nat. Rev. Dis. Primers *4*, 27.

28. Abbott, N.J. (2013). Blood-brain barrier structure and function and the challenges for CNS drug delivery. J. Inherit. Metab. Dis. *36*, 437–449.

29. Lim-Melia, E.R., and Kronn, D.F. (2009). Current enzyme replacement therapy for the treatment of lysosomal storage diseases. Pediatr. Ann. *38*, 448–455.

30. Barton, N.W., Furbish, F.S., Murray, G.J., Garfield, M., and Brady, R.O. (1990). Therapeutic response to intravenous infusions of glucocerebrosidase in a patient with Gaucher disease. Proc. Natl. Acad. Sci. USA *87*, 1913–1916.

31. Rombach, S.M., Smid, B.E., Linthorst, G.E., Dijkgraaf, M.G., and Hollak, C.E. (2014). Natural course of Fabry disease and the effectiveness of enzyme replacement therapy: a systematic review and meta-analysis: effectiveness of ERT in different disease stages. J. Inherit. Metab. Dis. *37*, 341–352.

32. Harmatz, P., Hendriksz, C.J., Lampe, C., McGill, J.J., Parini, R., Leão-Teles, E., Valayannopoulos, V., Cole, T.J., Matousek, R., Graham, S., et al.; MPS VI Study Group (2017). The effect of galsulfase enzyme replacement therapy on the growth of patients with mucopolysaccharidosis VI (Maroteaux-Lamy syndrome). Mol. Genet. Metab. *122*, 107–112.

33. Hendriksz, C.J., Burton, B., Fleming, T.R., Harmatz, P., Hughes, D., Jones, S.A., Lin, S.-P., Mengel, E., Scarpa, M., Valayannopoulos, V., et al.; STRIVE Investigators (2014). Efficacy and safety of enzyme replacement therapy with BMN 110 (elosulfase alfa) for Morquio A syndrome (mucopolysaccharidosis IVA): a phase 3 randomised placebo-controlled study. J. Inherit. Metab. Dis. *37*, 979–990.

34. Desnick, R.J., and Schuchman, E.H. (2012). Enzyme replacement therapy for lysosomal diseases: lessons from 20 years of experience and remaining challenges. Annu. Rev. Genomics Hum. Genet. *13*, 307–335.

35. Lund, T.C. (2013). Hematopoietic stem cell transplant for lysosomal storage diseases. Pediatr. Endocrinol. Rev. *11* (*Suppl 1*), 91–98.

36. Biffi, A. (2016). Gene therapy for lysosomal storage disorders: a good start. Hum. Mol. Genet. *25* (R1), R65–R75.

37. Nagree, M.S., Scalia, S., McKillop, W.M., and Medin, J.A. (2019). An update on gene therapy for lysosomal storage disorders. Expert Opin. Biol. Ther. *19*, 655–670.

38. Penati, R., Fumagalli, F., Calbi, V., Bernardo, M.E., and Aiuti, A. (2017). Gene therapy for lysosomal storage disorders: recent advances for metachromatic leukodystrophy and mucopolysaccaridosis I. J. Inherit. Metab. Dis. *40*, 543–554.

39. Sano, R., Tessitore, A., Ingrassia, A., and d'Azzo, A. (2005). Chemokine-induced recruitment of genetically modified bone marrow cells into the CNS of GM1-gangliosidosis mice corrects neuronal pathology. Blood *106*, 2259–2268.

40. Jeyakumar, M., Thomas, R., Elliot-Smith, E., Smith, D.A., van der Spoel, A.C., d'Azzo, A., Perry, V.H., Butters, T.D., Dwek, R.A., and Platt, F.M. (2003). Central nervous system inflammation is a hallmark of pathogenesis in mouse models of GM1 and GM2 gangliosidosis. Brain *126*, 974–987.

41. Pastores, G.M. (2010). Therapeutic approaches for lysosomal storage diseases. Ther. Adv. Endocrinol. Metab. *1*, 177–188.

42. Chen, J.C., Luu, A.R., Wise, N., Angelis, R., Agrawal, V., Mangini, L., Vincelette, J., Handyside, B., Sterling, H., Lo, M.J., et al. (2020). Intracerebroventricular enzyme replacement therapy with β-galactosidase reverses brain pathologies due to GM1 gangliosidosis in mice. J. Biol. Chem. *295*, 13532–13555.

43. Schulz, A., Ajayi, T., Specchio, N., de Los Reyes, E., Gissen, P., Ballon, D., Dyke, J.P., Cahan, H., Slasor, P., Jacoby, D., and Kohlschütter, A.; CLN2 Study Group (2018). Study of Intraventricular Cerliponase Alfa for CLN2 Disease. N. Engl. J. Med. *378*, 1898–1907.

44. Prada, C.E., Gonzaga-Jauregui, C., Tannenbaum, R., Penney, S., Lupski, J.R., Hopkin, R.J., and Sutton, V.R. (2014). Clinical utility of whole-exome sequencing in rare diseases: Galactosialidosis. Eur. J. Med. Genet. *57*, 339–344.

45. Darin, N., Kyllerman, M., Hård, A.L., Nordborg, C., and Månsson, J.E. (2009). Juvenile galactosialidosis with attacks of neuropathic pain and absence of sialyloligosaccharidуria. Eur. J. Paediatr. Neurol. *13*, 553–555.

46. Mosca, R., van de Vlekkert, D., Campos, Y., Fremuth, L.E., Cadaoas, J., Koppaka, V., Kakkis, E., Tifft, C., Toro, C., Allievi, S., et al. (2020). Conventional and Unconventional Therapeutic Strategies for Sialidosis Type I. J. Clin. Med. *9*, 695.

47. Bonten, E.J., Yogalingam, G., Hu, H., Gomero, E., van de Vlekkert, D., and d'Azzo, A. (2013). Chaperone-mediated gene therapy with recombinant AAV-PPCA in a new mouse model of type I sialidosis. Biochim. Biophys. Acta *1832*, 1784–1792.